Hindawi Publishing Corporation
Journal of Nanotechnology
Volume 2014, Article ID 381273, 9 pages
http://dx.doi.org/10.1155/2014/381273

Research Article

Binder Free SnO_2-CNT Composite as Anode Material for Li-Ion Battery

Dionne Hernandez,[1,2,3] Frank Mendoza,[2,3] Emmanuel Febus,[2,3] Brad R. Weiner,[2,3] and Gerardo Morell[2,4]

[1] *Photovoltaic and Electrochemical Systems Branch, NASA Glenn Research Center, LEX, 21000 Brookpark Road, Cleveland, OH 44135, USA*
[2] *Institute of Functional Nanomaterials, University of Puerto Rico, San Juan, PR 00931, USA*
[3] *Chemistry Department, University of Puerto Rico, San Juan, PR 00936, USA*
[4] *Physics Department, University of Puerto Rico, San Juan, PR 00936, USA*

Correspondence should be addressed to Dionne Hernandez; dmhernandezlugo@gmail.com

Received 26 November 2013; Revised 8 April 2014; Accepted 16 April 2014; Published 25 May 2014

Academic Editor: Valery Khabashesku

Tin dioxide-carbon nanotube (SnO_2-CNT) composite films were synthesized on copper substrates by a one-step process using hot filament chemical vapor deposition (HFCVD) with methane gas (CH_4) as the carbon source. The composite structural properties enhance the surface-to-volume ratio of SnO_2 demonstrating a desirable electrochemical performance for a lithium-ion battery anode. The SnO_2 and CNT interactions were characterized by X-ray diffraction (XRD), scanning electron microscopy (SEM), transmission electron microscopy (TEM), Raman spectroscopy, X-ray photoelectron spectroscopy (XPS), and Fourier transform infrared-attenuated total reflectance (ATR-FTIR) spectroscopy. Comprehensive analysis of the structural, chemical, and electrochemical properties reveals that the material consists of self-assembled and highly dispersed SnO_2 nanoparticles in CNT matrix. The process employed to develop this SnO_2-CNT composite film presents a cost effective and facile way to develop anode materials for Li-ion battery technology.

1. Introduction

Lithium-ion batteries (LIB) are one of the most popular types of chemistry for portable electronics with one of the best energy-to-weight ratios, no memory effect, and slow rate of self discharge. LIB cells involve transfer of electrons between two host materials of the anode (negative electrode) and the cathode (positive electrode) such that simultaneous redox reactions take place at both electrodes concurrent with insertion/deinsertion of Li cations. While graphite, which exhibits a theoretical capacity of 372 mAh/g, is the preferred anode used in commercial Li-ion batteries, considerable research has been conducted recently to identify different materials as possible alternative anodes exhibiting higher capacity and lower irreversibility. The limited capacity obtained on this commercial LIB moves researchers attention to materials (e.g., Si and Sn) that could deliver from 1000 and up to 4000 mAh/g specific capacity.

SnO_2 is being assessed as an anode material to replace the currently used graphite due to its high theoretical capacity, high conductivity, its thermal and mechanical stability in air, and low cost [1, 2]. Sn anodes reversible capacity is approximately 994 mAh/g (Sn) and 790 mAh/g (SnO_2) resulting in 4.4 Li for every Sn in comparison with graphite which exhibits a capacity of 372 mAh/g for the intercalation compound LiC_6 [3].

The implementation of Sn as an anode is limited by the volume expansion of approximately 259% when cycled causing pulverization and loss of electrical contact between individual particles thus resulting in severe capacity fading over time [4]. A method to minimize the volume expansion is to make the active material structure at the nanometer scale

as well as preserving the active material within a matrix constraining the volume change. Earlier, it was demonstrated that addition of 1D carbon nanotubes mitigates the expansion of tin resulting in good cycling capability of the tin-based composite [3]. Tin oxide-CNT composites have been prepared by chemical routes [5, 6], electrospinning [7, 8], and dual processes where the CVD is used to form the CNT followed by a chemical route [9]. Most recently, tin oxide in SnO_2-CNT composites was introduced by using CVD gases, such as acetylene and tin chloride ($SnCl_4$) [7]. Most of these processes are time consuming and are not environmentally friendly due to toxic ingredients and products.

The goal of this study was to demonstrate the one-step synthesis of a SnO_2-CNT composite by direct CVD growth on a copper substrate. The advantage of the proposed approach using direct deposition of the material on a Cu current collector substrate is in a binder free electrode. The carbon nanotubes serve as the buffering matrix to minimize the volume changes that take place during the alloying-dealloying and provide surface-to-volume ratio needed in transport of ions and electrons.

2. Experimental

2.1. Materials. Copper substrate (GoodFellow, 99.9%), nickel (II) oxide (Alfa Aesar, 99+%), tin oxide nanopowder (Nanostructured & Amorphous Materials, Inc., 99.5%), isopropyl alcohol (Fisher Scientific), ethyl alcohol (Sasma, 95%), and methane gas (Linde, 10% H_2) were used in this work.

2.2. Preparation of the Sample. Copper substrates of 0.5 mm thickness and 14 mm in diameter were polished using 600 to 2500 grit sand paper. After polishing, the substrates were ultrasonically cleaned for 5 minutes in isopropanol and dried in nitrogen. The catalyst dispersion for SnO_2-CNT growth was prepared by using SnO_2 nanoparticles and NiO in a 2 : 1 weight ratio dispersed in ethanol. Other ratios (e.g., 1 : 1, 1 : 2, and 10 : 1) did not lead to substantial CNT growth. The Ni-SnO_2 catalyst dispersion was deposited on the substrate surface on a hot plate and dried to form homogeneous coating. The standard CNTs were grown on copper using Ni as the catalyst. The Ni was deposited on the copper surface using the same process as previously described.

2.3. Synthesis of SnO_2-CNT Composite. The SnO_2-CNT composite films on copper substrates were grown in a custom made hot filament chemical vapor deposition (HFCVD) chamber, which has been previously described in detail elsewhere [10]. Prior to each deposition and before introducing methane, the CVD chamber was evacuated to 9×10^{-6} Torr. A mixture of 10% CH_4 in H_2 was used as the carbon source. The gas pressure was kept constant at 35 Torr during the deposition time of 5 minutes. The filament temperature was kept at $2500 \pm 25^{\circ}$C, the filament-substrate distance was 7.5 mm, and the substrate temperature was kept at $700 \pm 25^{\circ}$C. The surface and nanostructure of the composite films were analyzed by high resolution scanning electron microscopy (HRSEM) with a JEOL JSM-7500F.

2.4. Structural Characterization. The morphology of the SnO_2-CNT composite films was performed using field emission scanning electron microscope (FE-SEM) JEOL JSM-7500F and a Carl Zeiss TEM LEO 922 transmission electron microscope (TEM) operated at 200 kV. The TEM sample was prepared by scraping the composite from the Cu substrate into ethanol, depositing it on Cu grid, and drying. The SEM analysis was performed for bare CNT and SnO_2-CNT composite for comparison.

Raman spectra of the SnO_2-CNT composite films were obtained using a HORIBA Jobin Yvon T-64000 Raman spectrometer with a coherent argon-ion fluency laser operating with a 514.5 nm wavelength at a power density of 5 $kWcm^{-2}$ with the probing area of about 2 μm^2. The Raman spectra were obtained from 100 to 2000 cm^{-1}. This technique was used to determine the G and D bands for the CNTs in the composite films, as well as the I_G/I_D ratio, in order to establish the quality of the carbon nanotube structure.

X-ray photoelectron spectroscopy (XPS) was used to determine the chemical state of each element and organic residues that functionalize the CNT walls and affect chemical interactions with organic compounds or gas adsorption [11, 12]. XPS was carried out using a physical electronic 5600 X-ray photoelectron spectrometer. The analyses were performed at a base pressure of 5×10^{-9} Torr or lower. The Al Kα X-ray monochromatic source was operated at 350 W and 15 kV; the high resolution XPS survey spectra were performed from 187.85 eV to 29.35 eV. The take-off angle was 45°. Survey scans were performed in order to detect all the chemical elements present, and then high resolution scans were collected for C 1s, O 1s, Sn 3d, and Ni 2p signatures on the SnO_2-CNT composite films. All binding energies were corrected considering the aliphatic hydrocarbon C 1s contribution at 284.5 eV. The fitting of all spectra was performed with mixed Gaussian-Lorentzian distributions and iterated Shirley background lines using a multipack software.

FTIR spectroscopy was used to identify organic functional groups on a CNT surface by measuring characteristic vibrational modes. In this investigation, FTIR recording was carried out in the range of 400–4000 cm^{-1} to study and further characterize the SnO_2-CNT composite films. ATR-FTIR spectra of solid SnO_2-CNT sample were obtained using a Bruker Tensor 27 with a Helios ATR attachment.

X-ray diffraction (XRD) patterns were determined at room temperature at a scanning rate of 3θ/min. The XRD patterns were determined for the catalyst NiO : SnO_2 and the SnO_2-CNT composite films. The catalyst solution pattern was recorded in the 2θ range from 10° to 80°. The SnO_2-CNT composite film patterns were obtained from 20° to 70°. The analysis was done using a Rigaku Dmax-2200 X-ray diffractometer with Cu Kα radiation (1.5406 Å).

2.5. Electrochemical Characterization. The SnO_2-CNT composite samples were assembled in CR-2032 coin cells. The assembly process was performed in a glove box under a dry argon atmosphere. The binder free SnO_2-CNTs were used as negative working electrodes with lithium foil acting as both counter and reference electrode and Celgard 2400 as a

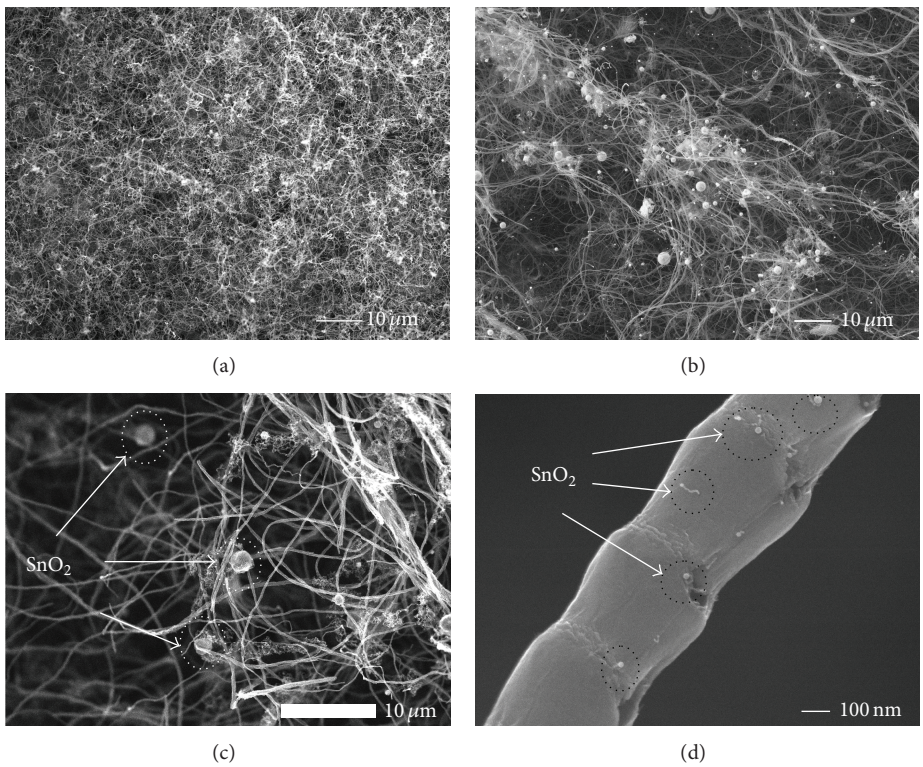

(a) (b) (c) (d)

Figure 1: Field emission scanning electron microscopy images of (a) CNT alone and (b)–(d) SnO_2-CNT composite. Circles in figures (c) and (d) indicate the location of the SnO_2 particles.

separator. The electrolyte was composed of 1.0 M $LiPF_6$ dissolved in ethylene carbonate (EC) and diethyl carbonate (DC) in a 1 : 1 volume ratio. Cyclic voltammetry was performed at a 0.1 mV/s scan rate over a potential range of 0.01 V to 2.00 V versus Li/Li^+. Charge-discharge measurements were performed between 0.01 and 3.00 V versus Li/Li^+ using a Gamry Potentiostat at room temperature; the mass of the electrode was determined by scraping the material from the copper substrate.

3. Results and Discussion

3.1. Materials Characterization. The SnO_2-CNT composite films were grown directly on copper substrates by one-step process, resulting in uniformly coated substrates without any cracks. Figure 1 shows SEM images of standard CNT (Figure 1(a)) and SnO_2-CNT composites (Figures 1(b), 1(c), and 1(d)). It is readily seen that the CNTs grow in a spaghetti-like structure and micron-size clusters of SnO_2 are dispersed among the CNTs (Figures 1(b) and 1(c)). A closer look at the CNT reveals that there are SnO_2 nanoparticles as clusters of SnO_2 particles embedded in the CNT matrix and dispersed on the outer walls of the CNT. The isolated SnO_2 nanoparticles (Figure 1(c)) have a particle size between 5 and 10 nm, and the clusters (Figure 1(d)) have a size range of 30–100 nm. Moreover, the CNTs have regularly spaced nodes resembling bamboo structures, or bamboo-like carbon nanotubes (BCNTs) [11]. The bamboo-like carbon nanotubes consist of diameters between 100 and 200 nm and more than 10 μm of length. The actual structure is more clearly seen in the TEM images (Figure 2(a)). By analyzing the TEM images in a closer scan (Figure 2(b)), we can see that the SnO_2 appear on the surface of the CNT as well as in CNT matrix making the CNT a buffering matrix. This composite structure is a direct consequence of the one-step growth process hereby employed, as opposed to sputtering, coating, or painting SnO_2 onto the CNT.

Raman spectroscopy was performed on the SnO_2-CNT sample to analyze the quality of the carbon nanotubes in the range of 1000–1800 cm^{-1} (Figure 3). The region contains the D and G bands at 1349 cm^{-1} and 1576 cm^{-1}, respectively. Well-defined peaks imply high quality of the grown CNT. The band at 1349 cm^{-1} corresponds to the D band which gives information on the degree of disordered sp^2 carbon present in the carbon nanotubes, and the G band at 1576 cm^{-1} corresponds to a splitting of the E_{2g} stretching mode of crystalline graphite. The G-to-D band intensity ratio (I_G/I_D) is 0.83. This value indicates that CNTs are significantly disordered in their periodic structure. The I_G/I_D ratio indicates the presence of amorphous carbon, which in our case could contribute to the D band intensity [13].

XPS was performed to further study the surface chemistry of the SnO_2-CNT composite films. In Figure 4(a), the survey scan of the SnO_2-CNT composite is presented. It shows the presence of C, O, Sn, Ni, and Cu, from the substrate. The main peaks for the SnO_2-CNTs composites are the following: 284 eV (C 1s), 531 eV (O 1s), 487 eV and 486 eV (Sn 3d), and 856.5 eV (Ni 2p) [14]. Since no spurious peaks are present,

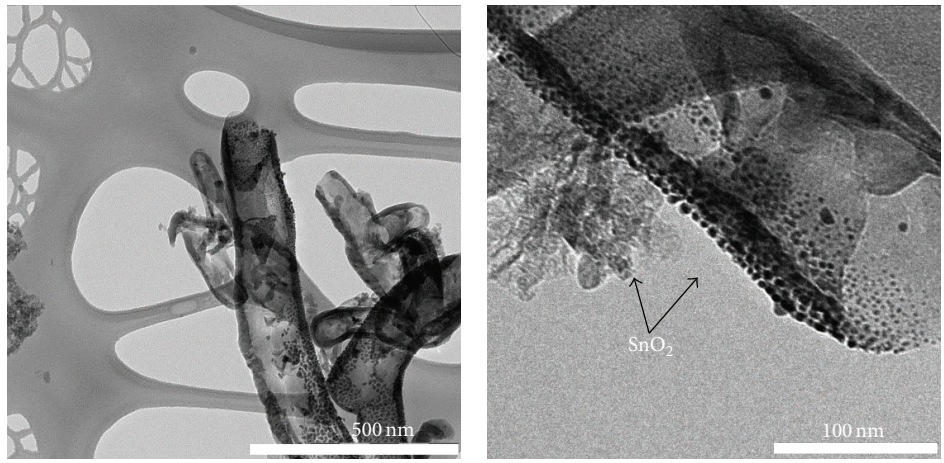

(a) (b)

Figure 2: Transmission electron microscopy images of SnO_2-CNT composite. (a) View of the composite structure and (b) higher magnification which shows the bamboo-like structure of the CNTs and the SnO_2 covered partially by the CNT.

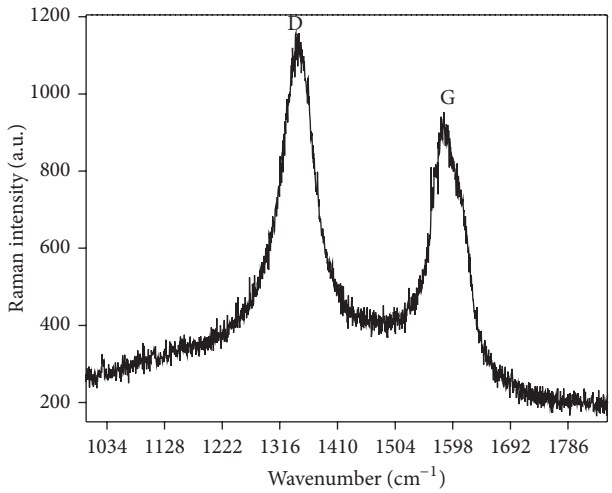

Figure 3: Raman spectrum for the as-grown SnO_2-CNT composite from 1000 to 1800 cm^{-1} showing the D and G bands typical of CNT.

the survey scan confirms the purity of the experimental setup for sample preparation procedure and nanostructure growth. Figures 4(b)–4(e) present the high resolution scans of the previously listed elements. Figure 4(b) shows the deconvolution of the C 1s spectrum, considering four band contributions at 284.4 eV, 285.2 eV, 287.8 eV, and 290.8 eV. The main C 1s line appears at 284.4 eV, which corresponds to the sp^2 C=C bond pyrolytic graphite [15, 16]. The peak at 285.2 eV corresponds to sp^3 carbon (C–C). The higher binding energy observed for sp^3 carbon compared to sp^2 ones suggests some disordering in the graphite structure [7, 15] which is in accordance with the Raman spectroscopy results. The peak at 287.8 eV has been reported as oxygen carbon (C–O) bonding, and it is possible to observe the carbon sp^2 shake-up peak at 290.8 eV [12, 17]. Figure 4(c) presents the high resolution scan for O 1s; the band is asymmetrical and has shoulders at higher binding energies. The deconvolution treatment of the O 1s peak resulted in three peaks at 529.5 eV, 531.4 eV, and 533.4 eV. The main peak for O 1s appears at 531.3 eV, and it has been related to hydroxide species [18]. The peak at 529.4 eV is due to oxygen metal bonding. This peak can be assigned to the presence of Sn and Ni oxides (M–O) [19]. The peak at 533.4 eV was assigned to oxygen adsorbed on the surface of the material [18, 19]. In Figure 4(d), the doublet for Sn $3d_{5/2}$ and Sn $3d_{3/2}$ is observed at 487.0 eV and 495.4 eV. The separation between these two peaks is about 8.4 eV, which is in good agreement with the energy splitting found in previous reports for tetragonal SnO_2 [7, 20, 21]. The NIST database [14] reports oxidizing states for tin as Sn^0 (485.0 eV), Sn^{2+} (485.9 eV), and Sn^{4+} (486.6 eV). The fitting of the Sn $3d_{5/2}$ peak (not shown) was performed with one component attributed to Sn^{4+}, which is in agreement with the presence of SnO_2 in the carbon nanotubes composite with a valence of 4+. There was no contribution to any other component which might have emerged from the deposition process. Figure 4(e) shows the peak corresponding to Ni 2p and demonstrates the presence of Ni used as a catalyst for CNT growth with a valence of 2+.

Figure 5 presents the XRD patterns for the Ni : SnO_2 catalyst before CVD process (a) and SnO_2-CNT composite film after the completion of the CVD process (b). The diffraction peaks corresponding to the Ni : SnO_2 catalyst before CVD process are found in Figure 5(a); here, we identified the patterns for tin oxide (IV), NiO, and Cu. The peaks at $2\theta = 26.97^\circ$, 33.97°, and 51.02° correspond to (1 1 0), (1 0 1), and (2 1 1) lattice planes of SnO_2, confirming the tetragonal rutile structure of tin oxide (IV). The peak corresponding to the NiO lattice plane can be observed at $2\theta = 37.40^\circ$. The peaks present at $2\theta = 44.29^\circ$, 50.40°, and 74.14° correspond to (1 1 1), (2 0 0), and (2 2 0) lattice planes of copper used as the material supporting substrate. The catalyst XRD patterns were analyzed for comparison with the patterns obtained in the SnO_2-CNT composite films.

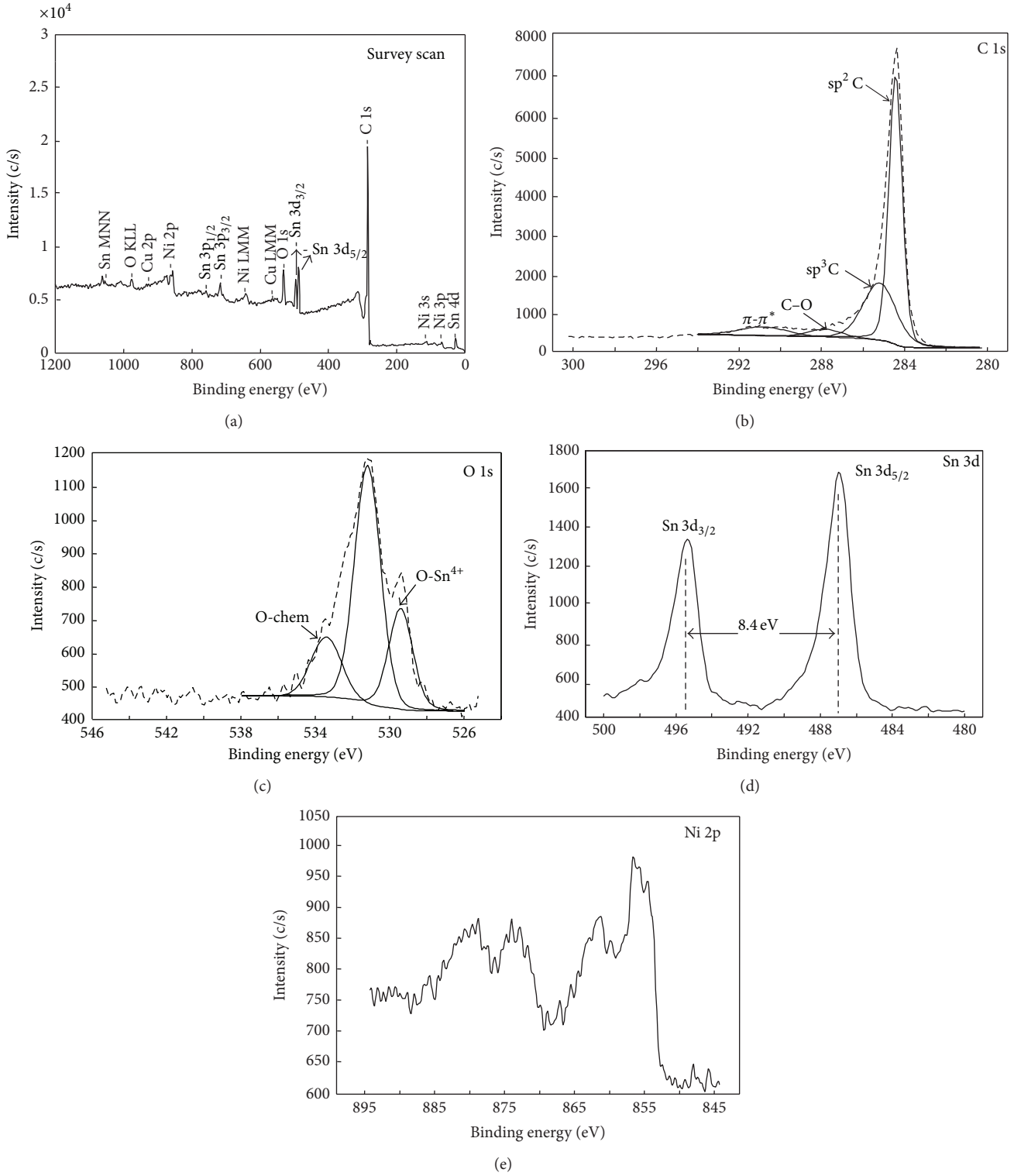

FIGURE 4: X-ray photoelectron spectroscopy spectrum of SnO_2-CNT composites: (a) survey scan; (b)–(e) deconvoluted spectra for (b) C 1s, (c) O 1s, (d) Sn 3d, and (e) Ni 2p. Experimental data are represented by dashed lines (- - -) and components contribution is represented by continuous line.

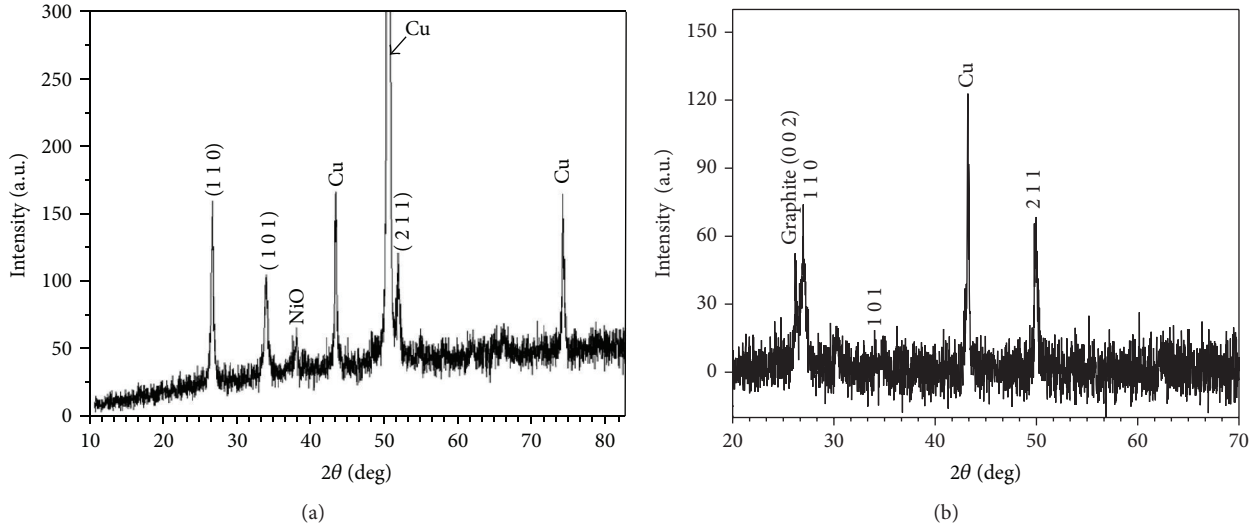

Figure 5: (a) X-ray diffractogram of Ni : SnO_2 catalyst dispersion. (b) SnO_2-CNT composite films. ((a), (b)) The three peaks characteristic of tetragonal SnO_2 are presented as follows: (1 1 0), (1 0 1), and (2 1 1). (b) The CNT pattern is labeled as (0 0 2).

The diffraction peaks for the SnO_2-CNT composites films are found in Figure 5(b). Here, the peak for CNT is observed at $2\theta = 26.19^\circ$, consistent with reference values of crystalline graphite [22]. In this figure, it is labeled as graphite (0 0 2). The relatively strong peaks observed at $2\theta = 26.97^\circ$, 33.95°, and 51.02° correspond to the (1 1 0), (1 0 1), and (2 1 1) lattice planes of SnO_2. The maximum diffraction peaks for the tetragonal SnO_2 are in good agreement with the values reported in the literature [8, 23, 24]. The main peak of tetragonal SnO_2 (1 1 0) has a higher intensity and is overlapping with the main peaks of graphite (0 0 2). The main peak corresponding to the (1 1 0) plane for SnO_2 is maintained after the heat treatment obtained as part of the CNT growth process; this is confirmed by observing the XRD diffraction patterns for the bare CNT. It has been reported that the temperature treatment could cause a structural change of tin in presence of nickel forming Ni_3Sn_4; in this study, there is no evidence of tin alloy compounds formed other than the carbon nanotube and tin-based composite [4]. The temperature used for this deposition in conjunction with short deposition time improves the purity of the composite material. As a result, no other tin compounds are observed in the SnO_2-CNT composite films. The observed XRD patterns confirm that no structural changes took place during the deposition process. The Cu peak observed on the SnO_2-CNT composite films XRD patterns originates from the substrate.

ATR-FTIR spectroscopy was used to determine the presence of CNTs and SnO_2 as well as determine the presence of any functional groups in the CNTs surface that might have emerged from the deposition process. The ATR-FTIR spectrum (Figure 6) indicates a small absorption peak in the 3500–3700 cm^{-1} range due to hydrogen-bonded oxygen (O–H) stretch vibrations [25]. The peaks in the 2760–3071 cm^{-1} region are attributed to asymmetric and symmetric C–H stretching bonds, respectively [26]. The peaks in the 1000–1080 cm^{-1} are due to the C–C and O–C stretch vibrations of the CNTs [7, 27]. The peak at 817 cm^{-1} is characteristic of O–Sn–O stretching modes [28]. The above analysis further confirms that the SnO_2 and CNTs are assembled into a composite, rather than heterostructure.

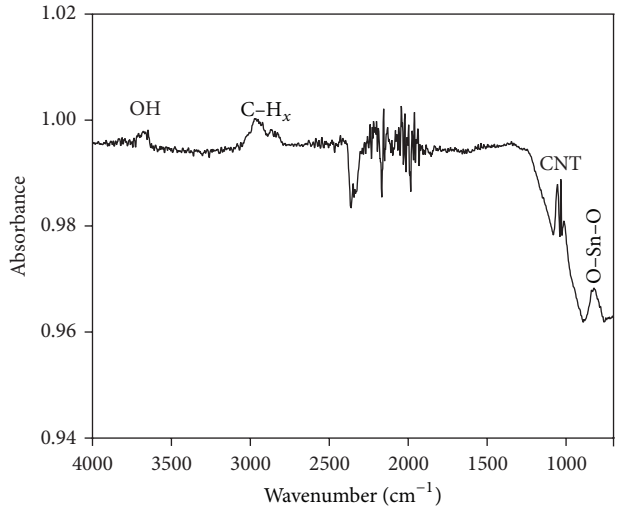

Figure 6: Characteristic attenuated total reflectance: Fourier transform infrared spectra of SnO_2-CNT composite.

3.2. Electrochemical Characterization. The cyclic voltammetry for the SnO_2-CNT composite can be seen in Figure 7(b). The electrochemical measurement allows distinguishing between reversible and irreversible processes that occur as part of the electrochemical process with Li ions. A number of peaks are observed characterizing the SnO_2-CNT composite interaction with Li ions in the first cathodic scan. The peak characteristic of lithium intercalation into carbon is observed at 0.01 V (4′), and the deintercalation of lithium from the

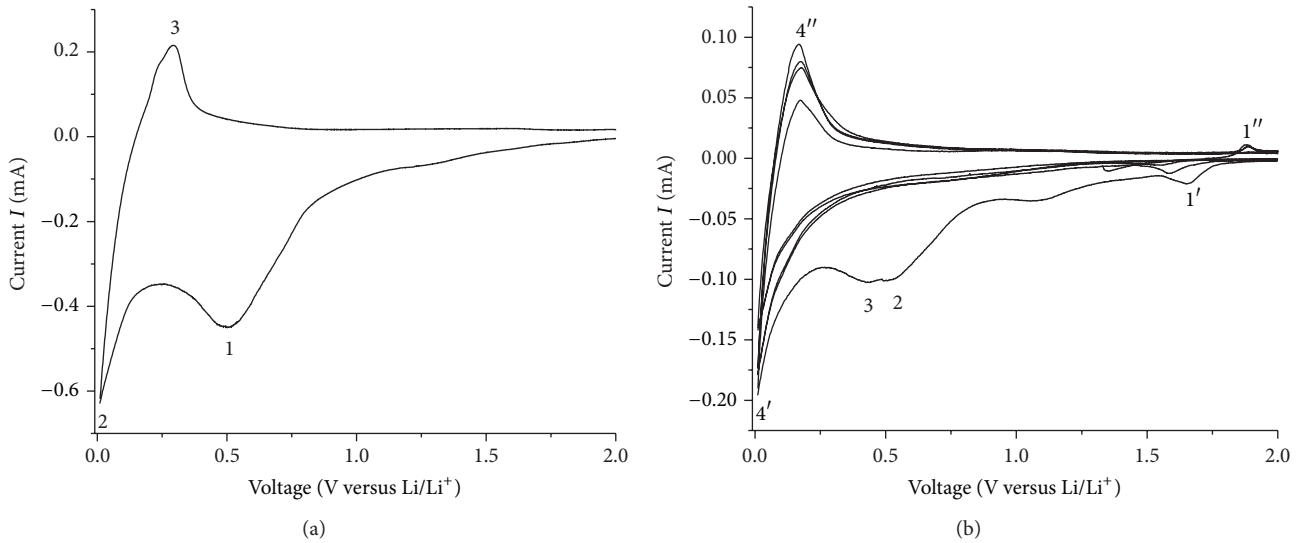

Figure 7: (a) Cyclic voltammetry of bare CNT film on copper at a scan rate of 0.10 mV/s. (b) Cyclic voltammetry of SnO_2-CNT composite film on copper at a scan rate of 0.10 mV/s.

carbon is observed at 0.20 V ($4''$); this is consistent in every cycle indicating that this process is reversible. The solid electrolyte interface (SEI) is formed on the surface of the carbon nanotubes, and this is observed at 0.80 Volts and 1.25 Volts (2); the interpretation is supported by the peak position whose value is typical for the formation of the solid electrolyte interface as reported by Jung et al. This is also supported by comparing it to the CV of the bare CNT (Figure 7(a)). The peak from 0.50 to 0.20 V (3) can be ascribed as the formation of the phases of tin with lithium Li_xSn as described in (2) [28]. The peak at 1.65 V ($1'$) is associated with the reduction of SnO_2 into metallic Sn as described in (1) [27, 28]. This peak is observed in the second cycle with a lower intensity and at a lower voltage. The anodic peak at 1.80 V ($1''$) appears after the first cycle and is thought to be related to the partially related reversible reaction of SnO_2 with Li [28, 29].

Tin oxide electrochemical behavior works on two-step processes:

$$4Li^+ + 4e^- + SnO_2 \longrightarrow 2Li_2O + Sn \quad (1)$$

$$Sn + xLi^+ + xe^- \longleftrightarrow Li_xSn \quad (0 \le x \le 4.4) \quad (2)$$

By observing the cyclic voltammetry for the SnO_2-CNT composite, we could see that the decomposition of the electrolyte occurs on the surface of the carbon nanotubes. This indicates that carbon nanotubes not only work as a buffering and conductive matrix but also perform as a host matrix for Li, increasing the composite overall capacity. Even though the carbon nanotubes and the tin oxide form a composite, they both interact independently with Li.

To confirm these findings, the CV measurements were performed on bare CNT to compare the interaction of these systems with the Li ions. The bare CNTs were prepared by the same process as the SnO_2-CNT using Ni in ethanol as the catalyst solution. In Figure 7(a), the cyclic voltammetry of bare CNT shows a peak characteristic of the electroactive carbon. Here, the peak corresponding to the intercalation of lithium into the CNT is observed at 0.01 V (2). The reversible process is characterized by the anodic peak at 0.20 V (3) corresponding to the deintercalation of lithium from CNT. The solid electrolyte interface (SEI) is observed at 0.80 V and 1.25 V (1), and this is due to the interaction of the electrolyte with the surface of the CNT [28]. This electrochemical characterization shows that Li interacts with the CNT and the SnO_2 only excluding contribution of other materials used as part of the deposition process.

The charge-discharge profile for this novel SnO_2-CNT composite material was determined at 0.2 mA in a voltage range of 0.01–3.00 V resulting in a charge-discharge profile typical for this type of system [4, 27, 28]. The first discharge capacity for SnO_2-CNT composite was of 1200 mAh/g and ending with a discharge capacity of about 1096 mAh/g after 10 cycles. The capacity calculation was determined by taking the total mass of the SnO_2-CNT composite material. By observing the shape of the first cycle (Figure 8(a)), we can see that the main process in this system occurs on the first discharge and is in accordance with the CV for this system (Figure 7(b)). Here, the first discharge cycle can be divided into three voltage regions: (1) 0.01–0.6 V, (2) 0.6–1.3 V, and (3) 1.3–3.0 V. The area between 1.3 and 3.0 V is due to the reduction of SnO_2 to Sn. The SEI formation can be identified between 0.6 and 1.3 V, and the formation of the Li alloy phases with tin is observed at 0.01 to 0.6 V. It was observed that the first discharge graph reach 0.30 V; this did not affect the consecutive discharge process.

On this material, the carbon nanotube loading is higher than that of tin oxide. The loading for tin on the composite is of approximately 20 wt% determined by TGA (data not shown), and previously it has been reported that similar loadings have increased battery performance due to the introduction of a large carbon nanotube matrix covering the tin oxide from the electrolyte allowing the electrode contact area to be maintained [4, 28]. The SnO_2-CNT composite material demonstrated an enhanced first discharge capacity of

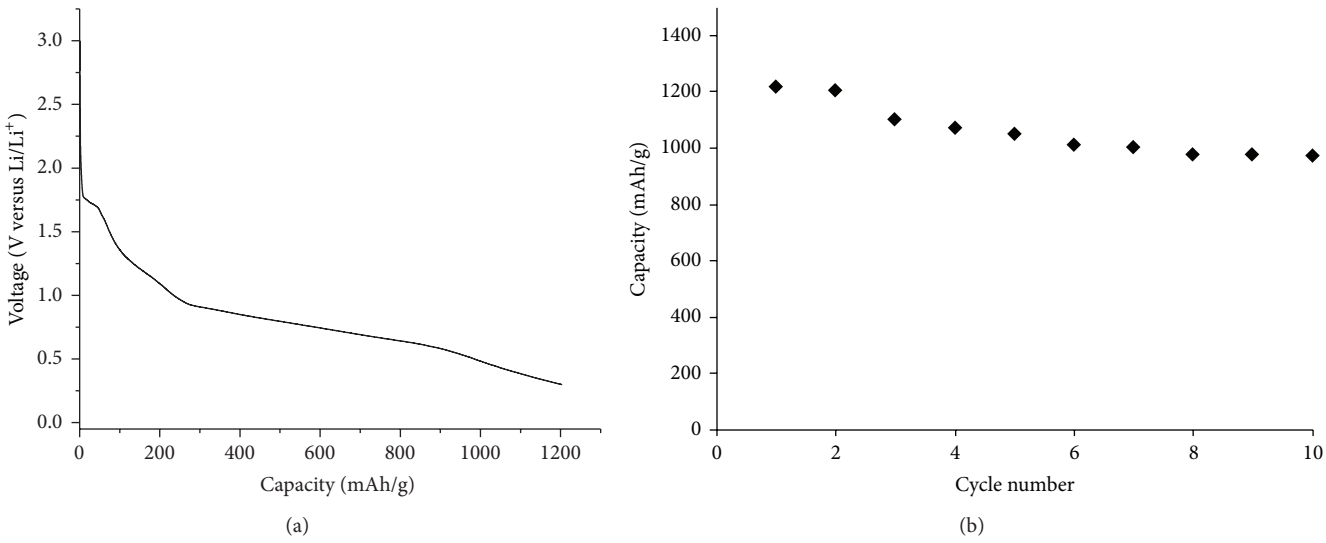

Figure 8: (a) First discharge of SnO_2-CNT composite. (b) Electrochemical properties of SnO_2-CNT composite during the first 10 cycles.

1200 mAh/g and a charge capacity of 200 mAh/g. This small charge capacity could be attributed to the formation of the SEI on the surface of the electrode. This decomposition of the electrolyte is involved in the first initial cycles and forms a covering film which consumes Li ions leading to a decrease in reversible capacity [1]. On the second charge/discharge cycle, the SnO_2-CNT composite delivered a reversible capacity with 90% capacity retention. In Figure 8(b), the performance of the first 10 cycles is presented.

4. Conclusions

We successfully report novel SnO_2-CNT composite films synthesized with a simple, cost effective, and environmentally friendly one step process. The composites were grown directly on copper substrates by means of a hot filament chemical vapor deposition technique, which utilizes methane as the only carbon source. An optimized SnO_2-CNT composite film self-assembled into tin dioxide nanoparticles in the outer wall of the CNT and micro SnO_2 particles in the CNT matrix were confirmed by SEM and TEM. The multilateral characterizations carried out on the materials show that they consist of tetrahedral SnO_2 nanoparticles arranged both on the CNT wall and throughout the CNT matrix with a small amount of amorphous carbon. The highly dispersed SnO_2-CNT matrix was analyzed as a lithium ion battery anode resulting in a discharge capacity of approximately 1000 mAh/g for 10 cycles.

Conflict of Interests

The authors declare that there is no conflict of interests regarding the publication of this paper.

Acknowledgments

Dionne Hernandez gratefully acknowledges the financial support from NASA Harriet-Jenkins Pre-doctoral Program (Grant no. NNX10AU20A). This research project was carried out under the auspices of the Institute for Functional Nanomaterials (NSF Grant no. 1002410). This research was also supported in part by PR NASA EPSCoR (NNX13AB22A) and PR NASA Space Grant (NNX10AM80H). The authors gratefully acknowledge the instrumentation and technical support of the Materials Characterization Center of the University of Puerto Rico with the ATR-FTIR and XPS (Dr. E. Facchini), the Raman Facility (Dr. R. S. Katiyar), and XRD (G. García) analysis. The authors would also like to thank Dr. Alevtina Smirnova for her suggestions on the paper.

References

[1] L. Ji, Z. Tan, T. Kuykendall et al., "Multilayer nanoassembly of Sn-nanopillar arrays sandwiched between graphene layers for high-capacity lithium storage," *Energy and Environmental Science*, vol. 4, no. 9, pp. 3611–3616, 2011.

[2] F. Cheng, Z. Tao, J. Liang, and J. Chen, "Template-directed materials for rechargeable lithium-ion batteries," *Chemistry of Materials*, vol. 20, no. 3, pp. 667–681, 2008.

[3] M. H. Chen, Z. C. Huang, G. T. Wu, G. M. Zhu, J. K. You, and Z. G. Lin, "Synthesis and characterization of SnO-carbon nanotube composite as anode material for lithium-ion batteries," *Materials Research Bulletin*, vol. 38, no. 5, pp. 831–836, 2003.

[4] X. Li, Y. Zhong, M. Cai et al., "Tin-alloy heterostructure encapsulated in amorphous carbon nanotubes as hybrid anodes in recheargeable lithium ion batteries," *Electrochimica Acta*, vol. 89, pp. 387–393, 2013.

[5] P. Wu, N. Du, H. Zhang, J. Yu, Y. Qi, and D. Yang, "Carbon-coated SnO_2 nanotubes: template-engaged synthesis and their application in lithium-ion batteries," *Nanoscale*, vol. 3, no. 2, pp. 746–750, 2011.

[6] K. C. Ng, S. Zhang, C. Peng, and G. Z. Chen, "Individual and bipolarly stacked asymmetrical aqueous supercapacitors of CNTs/SnO_2 and CNTs/MnO_2 nanocomposites," *Journal of the Electrochemical Society*, vol. 156, no. 11, pp. A846–A853, 2009.

[7] J. Mu, B. Chen, Z. Guo et al., "Tin oxide (SnO_2) nanoparticles/electrospun carbon nanofibers (CNFs) heterostructures: controlled fabrication and high capacitive behavior," *Journal of Colloid and Interface Science*, vol. 356, no. 2, pp. 706–712, 2011.

[8] C. A. Bonino, L. Ji, Z. Lin, O. Toprakci, X. Zhang, and S. A. Khan, "Electrospun carbon-tin oxide composite nanofibers for use as lithium ion battery anodes," *ACS Applied Materials and Interfaces*, vol. 3, no. 7, pp. 2534–2542, 2011.

[9] A. L. M. Reddy and S. Ramaprabhu, "Nanocrystalline metal oxides dispersed multiwalled carbon nanotubes as supercapacitor electrodes," *Journal of Physical Chemistry C*, vol. 111, no. 21, pp. 7727–7734, 2007.

[10] S. Gupta, B. L. Weiss, B. R. Weiner, and G. Morell, "Study of the electron field emission and microstructure correlation in nanocrystalline carbon thin films," *Journal of Applied Physics*, vol. 89, no. 10, pp. 5671–5677, 2001.

[11] C. Morant, J. Andrey, P. Prieto, D. Mendiola, J. M. Sanz, and E. Elizalde, "XPS characterization of nitrogen-doped carbon nanotubes," *Physica Status Solidi (A) Applications and Materials Science*, vol. 203, no. 6, pp. 1069–1075, 2006.

[12] K. A. Wepasnick, B. A. Smith, J. L. Bitter, and D. Howard Fairbrother, "Chemical and structural characterization of carbon nanotube surfaces," *Analytical and Bioanalytical Chemistry*, vol. 396, no. 3, pp. 1003–1014, 2010.

[13] R. Saito, M. Hofmann, G. Dresselhaus, A. Jorio, and M. S. Dresselhaus, "Raman spectroscopy of graphene and carbon nanotubes," *Advances in Physics*, vol. 60, pp. 413–550, 2011.

[14] http://srdata.nist.gov/xps/.

[15] H. Wang, A. Zhou, F. Peng, H. Yu, and J. Yang, "Mechanism study on adsorption of acidified multiwalled carbon nanotubes to Pb(II)," *Journal of Colloid and Interface Science*, vol. 316, no. 2, pp. 277–283, 2007.

[16] M. Li, M. Boggs, T. P. Beebe, and C. P. Huang, "Oxidation of single-walled carbon nanotubes in dilute aqueous solutions by ozone as affected by ultrasound," *Carbon*, vol. 46, no. 3, pp. 466–475, 2008.

[17] T. I. T. Okpalugo, P. Papakonstantinou, H. Murphy, J. McLaughlin, and N. M. D. Brown, "High resolution XPS characterization of chemical functionalised MWCNTs and SWCNTs," *Carbon*, vol. 43, no. 1, pp. 153–161, 2005.

[18] G. X. Zhang, S. H. Sun, D. Q. Yang, J. P. Dodelet, and S. Edward, "The surface analytical characterization of carbon fibers functionalized by H2SO4/HNO3 treatment," *Carbon*, vol. 46, no. 2, pp. 196–205, 2008.

[19] M. Kwoka, L. Ottaviano, M. Passacantando, S. Santucci, G. Czempik, and J. Szuber, "XPS study of the surface chemistry of L-CVD SnO_2 thin films after oxidation," *Thin Solid Films*, vol. 490, no. 1, pp. 36–42, 2005.

[20] Y. Wang and T. Chen, "Nonaqueous and template-free synthesis of Sb doped SnO_2 microspheres and their application to lithium-ion battery anode," *Electrochimica Acta*, vol. 54, no. 13, pp. 3510–3515, 2009.

[21] L. Yan, J. S. Pan, and C. K. Ong, "XPS studies of room temperature magnetic Co-doped SnO_2 deposited on Si," *Materials Science and Engineering B*, vol. 128, no. 1-3, pp. 34–36, 2006.

[22] X. Meng, Y. Zhong, Y. Sun, M. N. Banis, R. Li, and X. Sun, "Nitrogen-doped carbon nanotubes coated by atomic layer deposited SnO_2 with controlled morphology and phase," *Carbon*, vol. 49, no. 4, pp. 1133–1144, 2011.

[23] N. van Hieu, N. A. P. Duc, T. Trung, M. A. Tuan, and N. D. Chien, "Gas-sensing properties of tin oxide doped with metal oxides and carbon nanotubes: a competitive sensor for ethanol and liquid petroleum gas," *Sensors and Actuators B*, vol. 144, no. 2, pp. 450–456, 2010.

[24] D. Chen and L. Gao, "Novel synthesis of well-dispersed crystalline SnO_2 nanoparticles by water-in-oil microemulsion-assisted hydrothermal process," *Journal of Colloid and Interface Science*, vol. 279, no. 1, pp. 137–142, 2004.

[25] Z. Chen, J. K. L. Lai, C. H. Shek, and H. Chen, "Synthesis and structural characterization of rutile SnO_2 nanocrystals," *Journal of Materials Research*, vol. 18, no. 6, pp. 1289–1292, 2003.

[26] L. Zhang, V. U. Kiny, H. Peng et al., "Sidewall functionalization of single-walled carbon nanotubes with hydroxyl group-terminated moieties," *Chemistry of Materials*, vol. 16, no. 11, pp. 2055–2061, 2004.

[27] M. Winter and J. O. Besenhard, "Electrochemical lithiation of tin and tin-based intermetallics and composites," *Journal of Power Source*, vol. 173, pp. 965–971, 2007.

[28] Y. S. Jung, K. T. Lee, J. H. Ryu, D. Im, and S. M. Oh, "Sn-carbon core-shell powder for anode in lithium secondary batteries," *Journal of the Electrochemical Society*, vol. 152, no. 7, pp. A1452–A1457, 2005.

[29] M. Mohamedi, S. J. Lee, D. Takahashi, M. Nishizawa, T. Itoh, and I. Uchida, "Amorphous tin oxide films: preparation and characterization as an anode active material for lithium ion batteries," *Electrochimica Acta*, vol. 46, no. 8, pp. 1161–1168, 2001.